ADVANCES IN ATMOSPHERIC SCIENCES, VOL. 35, FEBRUARY 2018, 146–157

• **Original Paper** •

Comparison between MODIS-derived Day and Night Cloud Cover and Surface Observations over the North China Plain

Xiao ZHANG[1,3], Saichun TAN[*1,2], and Guangyu SHI[1]

[1] *State Key Laboratory of Numerical Modeling of Atmospheric Sciences and Geophysical Fluid Dynamics, Institute of Atmospheric Physics, Chinese Academy of Sciences, Beijing* 100029*, China*

[2] *Collaborative Innovation Center on Forecast and Evaluation of Meteorological Disasters, Nanjing University of Information Science and Technology, Nanjing* 210044*, China*

[3] *University of Chinese Academy of Sciences, Beijing* 100049*, China*

(Received 31 March 2017; revised 14 August 2017; accepted 9 October 2017)

ABSTRACT

Satellite and human visual observation are two of the most important observation approaches for cloud cover. In this study, the total cloud cover (TCC) observed by MODIS onboard the Terra and Aqua satellites was compared with Synop meteorological station observations over the North China Plain and its surrounding regions for 11 years during daytime and 7 years during nighttime. The Synop data were recorded eight times a day at 3-h intervals. Linear interpolation was used to interpolate the Synop data to the MODIS overpass time in order to reduce the temporal deviation between the satellite and Synop observations. Results showed that MODIS-derived TCC had good consistency with the Synop observations; the correlation coefficients ranged from 0.56 in winter to 0.73 in summer for Terra MODIS, and from 0.55 in winter to 0.71 in summer for Aqua MODIS. However, they also had certain differences. On average, the MODIS-derived TCC was 15.16% higher than the Synop data, and this value was higher at nighttime (15.58%–16.64%) than daytime (12.74%–14.14%). The deviation between the MODIS and Synop TCC had large seasonal variation, being largest in winter (29.53%–31.07%) and smallest in summer (4.46%–6.07%). Analysis indicated that cloud with low cloud-top height and small cloud optical thickness was more likely to cause observation bias. Besides, an increase in the satellite view zenith angle, aerosol optical depth, or snow cover could lead to positively biased MODIS results, and this affect differed among different cloud types.

Key words: cloud cover, MODIS, cloud-top height, cloud optical thickness, aerosol optical depth, view zenith angle

Citation: Zhang, X., S. C. Tan, and G. Y. Shi, 2018: Comparison between MODIS-derived day and night cloud cover and surface observations over the North China Plain. *Adv. Atmos. Sci.*, **35**(2), 146–157, https://doi.org/10.1007/s00376-017-7070-x.

1. Introduction

Clouds are an important element in climate dynamics, atmospheric radiation, as well as atmospheric physics (Warren et al., 2007). Clouds can strongly affect the radiation balance of Earth, as they have a cooling effect due to the enhancement of planetary albedo and a heating effect resulting from the greenhouse effect of clouds (Ramanathan et al., 1989). The cloud fraction reflects the cloud's spatial domain and is a crucial factor in energy exchange in the climate system (Lu et al., 2015). Thus, it is essential to detect the spatial distribution and temporal variation of total cloud cover (TCC).

Ground-based observation and satellite remote sensing are the two most commonly used cloud observation methods and have high spatial coverage and long time series (Lu et al., 2015). Ground-based observation includes human visual observations and ground-based automatic cloud detection (Kazantzidis et al., 2012). Since ground-based automatic cloud detection is restricted by short time series and low spatial coverage, human visual observation is still the most important source of cloud information (Kotarba, 2009; Feister et al., 2010; Huo and Lu, 2012; Lu et al., 2015). Visual observation is conducted at meteorological stations, which are also called Synop stations. This is the most traditional observation approach to obtain long-term cloud fraction data, and offers a relatively dense spatial coverage.

Satellite remote sensing is another important observation approach to obtain cloud fraction data. Compared with Synop observations, satellite data are not influenced by subjective factors. This observation method also provides the opportunity to obtain continuous and spatially uniform observations of cloud conditions (Kästner et al., 2004; Fontana et al., 2013). Nevertheless, the data quality varies with the different characteristics of satellites, such as the spectral, spatial and temporal resolution of the sensors (Fontana et al., 2013). In

* Corresponding author: Saichun TAN
Email: sctan@mail.iap.ac.cn

recent decades, satellite remote sensing has been developing rapidly and is considered to be the most important method of remote sensing in cloud detection. The MODIS instrument, onboard the Aqua and Terra satellites, is a passive imager with 36 spectral channels and a spatial resolution of 250 to 1000 m. Previous studies have shown that MODIS has higher cloud recognition capabilities, as well as better calibration and geometry, compared with other operational sensors (Platnick et al., 2003; Lu et al., 2015). Comparisons between MODIS and other satellites have indicated that the observational quality of MODIS represents an improvement over ISCCP and AVHRR (Heidinger et al., 2002; Kotarba, 2015).

Satellite-derived TCC has been compared with visual surface observations (Meerkötter et al., 2004; Kotarba, 2009; Fontana et al., 2013; Ma et al., 2014; Lu et al., 2015) and ground-based instruments (Key et al., 2004; An and Wang, 2015) in different regions of the world. The results show good consistency between satellite and surface observations in some regions (Kästner et al., 2004; Meerkötter et al., 2004), but also that MODIS tends to overestimate the cloud cover when compared with the surface observations in other regions (Kotarba, 2009; Fontana et al., 2013). The satellite-observed TCC is generally higher in winter and lower in summer, as determined from the observations of ISCCP, AVHRR and MODIS (Rossow et al., 1993; Kästner et al., 2004; Kotarba, 2009). Meerkötter et al. (2004) pointed out that, in areas with serious haze pollution in the Mediterranean, the satellite-observed cloud cover is much higher than in clean areas. Research in China has shown that the consistency between satellite and visual-surface-observed TCC is probably affected by air pollution and snow cover (Lu et al., 2015). Also, the cloud cover from satellite and surface observations has been reported to show greater deviation over the North China Plain (NCP) compared with other regions (Ma et al., 2014).

The NCP is an area with serious air pollution. Rapid economic growth over the past three decades has resulted in severe atmospheric pollution and frequent haze events (Che et al., 2014; Chen and Wang, 2015; Li, 2016). The aggravated pollution is accompanied by high aerosol loading levels (Qiu and Yang, 2000; Luo et al., 2001; Li et al., 2013; Zhang et al., 2013) and reductions in visibility (Che et al., 2007) and solar radiation (Che et al., 2005; Liang and Xia, 2005; Xia, 2010). In regions with high aerosol optical depth(AOD), the so-called shadowing effect caused by aerosols will lead to a smaller Synop-detected value of cloud fraction compared with the true value (Lu et al., 2015). Another important affect caused by high AOD is that MODIS tends to misjudge aerosol plumes as cloud in regions with heavy aerosol concentrations (Shang et al., 2014; Mao et al., 2015). However, comparisons between satellite and visual surface observations are still rare over areas with high atmospheric pollution like the NCP, particularly over the long term and in recent high-haze years.

In this paper, we present a detailed comparison of MODIS cloud cover data with Synop observations over the NCP and its surrounding regions during the period from December 2002 to November 2013 in daytime, and December 2002 to November 2009 at nighttime. We assess the discrepancies between the two datasets over high haze pollution regions and analyze these discrepancies with respect to cloud with different cloud-top heights (CTHs) and cloud optical thicknesses (COTs). The possible factors (particularly in terms of aerosol) related to the discrepancies between MODIS and Synop data are discussed for different cloud types.

2. Data and methods

Eleven years (December 2002 to November 2013) of MODIS-derived TCC and Synop TCC data during daytime and seven years (December 2002 to November 2009) during nighttime were used to analyze the observational consistency of the two datasets over the NCP and its surrounding regions. Five provinces (Liaoning, Hebei, Shandong, Shanxi and Henan) and two municipalities (Beijing and Tianjin) were chosen as the research area, as shown in Fig. 1a, because there is a high AOD center and frequent haze pollution during winter over these regions (Wang et al., 2015a, 2015b, 2015c, 2015d).

2.1. *Cloud fraction from MODIS*

The satellite-observed TCC was derived from MODIS onboard the Terra and Aqua satellites, which passes over each region of the world twice a day in daytime and at nighttime. For Terra, the overpass time is around 1130 LST (Local Standard Time, UTC+8) during the daytime and 2330 LST at nighttime. For Aqua, meanwhile, the overpass time is around 1330 LST during daytime and 0130 LST at nighttime. The MODIS collection 6 MYD06/MOD06 and MYDATML2/MODATML2 cloud and aerosol products were used, downloaded from the Level 1 and Atmospheric Archive and Distribution System (http://ladsweb.nascom.nasa.gov/). The cloud detection results were recorded into 1-km (at nadir) spatial resolution MODIS cloud mask. According to the cloudiness likelihood of a given pixel, it was labeled as "cloudy", "uncertain—probably cloudy", "probably clear" or

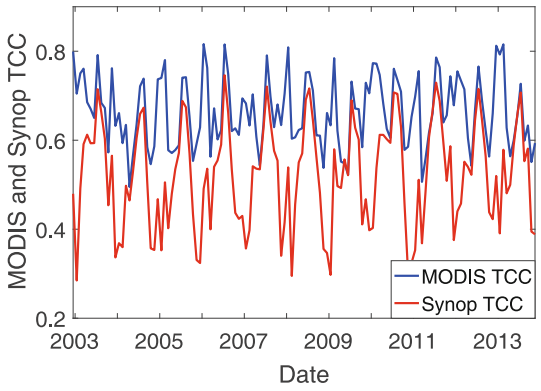

Fig. 1. Monthly mean TCC of 121 Synop stations observed by MODIS and Synop stations during daytime from December 2003 to November 2013.

"confidently clear". The first two conditions were regarded as cloudy and the latter two as clear when calculating the cloud fraction (Platnick et al., 2003). The cloud mask product was generated into cloud fractions at 5-km resolution by calculating the proportion of cloudy pixels from every 25-pixel cloud mask group (Menzel et al., 2008).

For comparison of satellite and surface observations, the usual approach is to average the satellite-derived cloud fraction or cloud mask data within the field of view (FOV) of the surface observation. Previous studies have found that a FOV with a radius of 30 or 35 km agrees better with the observers' FOV at each Synop station (Minnis et al., 2003; Meerkötter et al., 2004; Dybbroe et al., 2005; Fontana et al., 2013). In China, studies have found that satellite and surface observations correlate best when using a FOV with a 35-km radius (Lu et al., 2015). At each Synop station, we calculated the average MODIS cloud fraction within the surrounding 35-km radius to obtain the MODIS-observed TCC from Terra and Aqua, separately.

2.2. *Cloud fraction from surface data*

The surface TCC data are visual estimations of cloud cover and cloud type produced by observers at meteorological observation stations, which are sited in open areas away from buildings and trees in order to ensure the FOV is unaffected. The data were provided by the China Meteorological Sharing Service System (CMDSSS, 2016). In total, 121 Synop stations were chosen in the research area. Synop observations were performed at eight times a day at 3-h intervals—at 0200, 0500, 0800, 1100, 1400, 1700, 2000 and 2300 LST. To minimize the effect of the time differences between Synop and MODIS observations, possible approaches include choosing the Synop TCC nearest to the MODIS overpass time (Lu et al., 2015), calculating the average of two time points adjacent to the MODIS overpass time (Fontana et al., 2013), and interpolating the Synop TCC to the MODIS overpass time (Kotarba, 2009). In this study, the Synop TCC at three times nearest the overpass time (0800, 1100 and 1400 LST during daytime and 2000, 2300 and 0200 LST at nighttime for Terra; 1100, 1400 and 1700 LST during daytime and 2300, 0200 and 0500 at nighttime for Aqua) were interpolated to the satellites' overpass times with linear interpolation in order to reduce the errors caused by observational time deviation.

In terms of the dark conditions at nighttime seriously influencing the accuracy of visual surface observations (Minnis et al., 2003), the main existing method is to choose observations made at illuminations greater than that from a half-moon at zenith. The illumination of the moonlight from the lunar altitude and phase can be determined by the ephemeris and date (Hahn et al., 1992). The Extended Edited Cloud Report Archive (EECRA) is a dataset compiled based on global surface observation datasets. EECRA offers the relative lunar illuminance and flags denoting sufficient illumination from moonlight, twilight, or sunlight during the period 1971 to 2009 for land-based stations. In this study, 81 stations in or near the research area were chosen. For each Synop station to be compared, the nearest EECRA station was identified and their illuminations considered to be approximately equal.

Synop observations of cloud types divide the cloud at three levels into 10 types, separately. For the sake of analysis of cloud with different forms, we redivided clouds into 10 categories following the classification method defined by the International Meteorological Organization. The 10 cloud types were: cumulus cloud (Cu), cumulonimbus cloud (Cb), stratocumulus cloud (Sc) stratocumulus cloud (St), nimbostratus cloud (Ns), altostratus cloud (As), altocumulus cloud (Ac), cirrus cloud (Ci), cirrostratus cloud (Cs), and cirrocumulus cloud (Cc).

2.3. *Auxiliary data sets*

For the analysis of the factors influencing observations, five auxiliary datasets of CTH, COT, AOD at 550nm, satellite view zenith angle (VZA), and snow cover, were used. All were derived from Terra and Aqua MODIS Collection 6 data products. The AOD data were derived from the Deep Blue (DB) and Dark Target (DT) combined algorithm, and only the highest quality flag (QF=3) AOD data were used. The DT algorithm was developed to detect AOD over dark surfaces such as vegetation and ocean (Remer et al., 2005; Levy et al., 2007a, 2007b). In contrast, the DB algorithm can retrieve AOD over bright surfaces such as desert and snow (Hsu et al., 2004; Bilal and Nichol, 2015). The DT/DB algorithm is a "best of" AOD product with a wide coverage and high precision (Green et al., 2009; Levy et al., 2013; Bilal and Nichol, 2015). The snow cover data were derived from the MODIS snow and sea ice products MOD10/MYD10, which provide the snow cover and ice cap at a 0.05° resolution (Hall et al., 2006). All these auxiliary data were averaged within the same FOV, like the TCC.

3. Results and discussion

3.1. *Climatology of TCC from Aqua MODIS and Synop observations*

In order to realize the overall distribution of MODIS- and Synop-observed TCC, we first calculated the climatic field as well as the temporal variation of the TCC. As shown in Fig. 1, the cloud fraction showed distinct seasonal changes. The TCC observed by MODIS was generally greater than that from the Synop observations. The latter showed the lowest TCC in winter and highest in summer, yet the MODIS value was high both in summer and winter, and relatively low in spring and winter. The TCC observed by the two methods showed best consistency in summer and greatest deviation in winter. Analysis of the TCC climatic field is shown in Fig. 2. In general, the TCC of the southern part was higher than the northern part, which was roughly the same for MODIS and Synop observations. Meanwhile, it is notable that in winter the MODIS-observed TCC in the northern part was much larger than the Synop observation during daytime, while at nighttime both the MODIS- and Synop-derived TCC showed low values. In the southern part, the MODIS-observed TCC

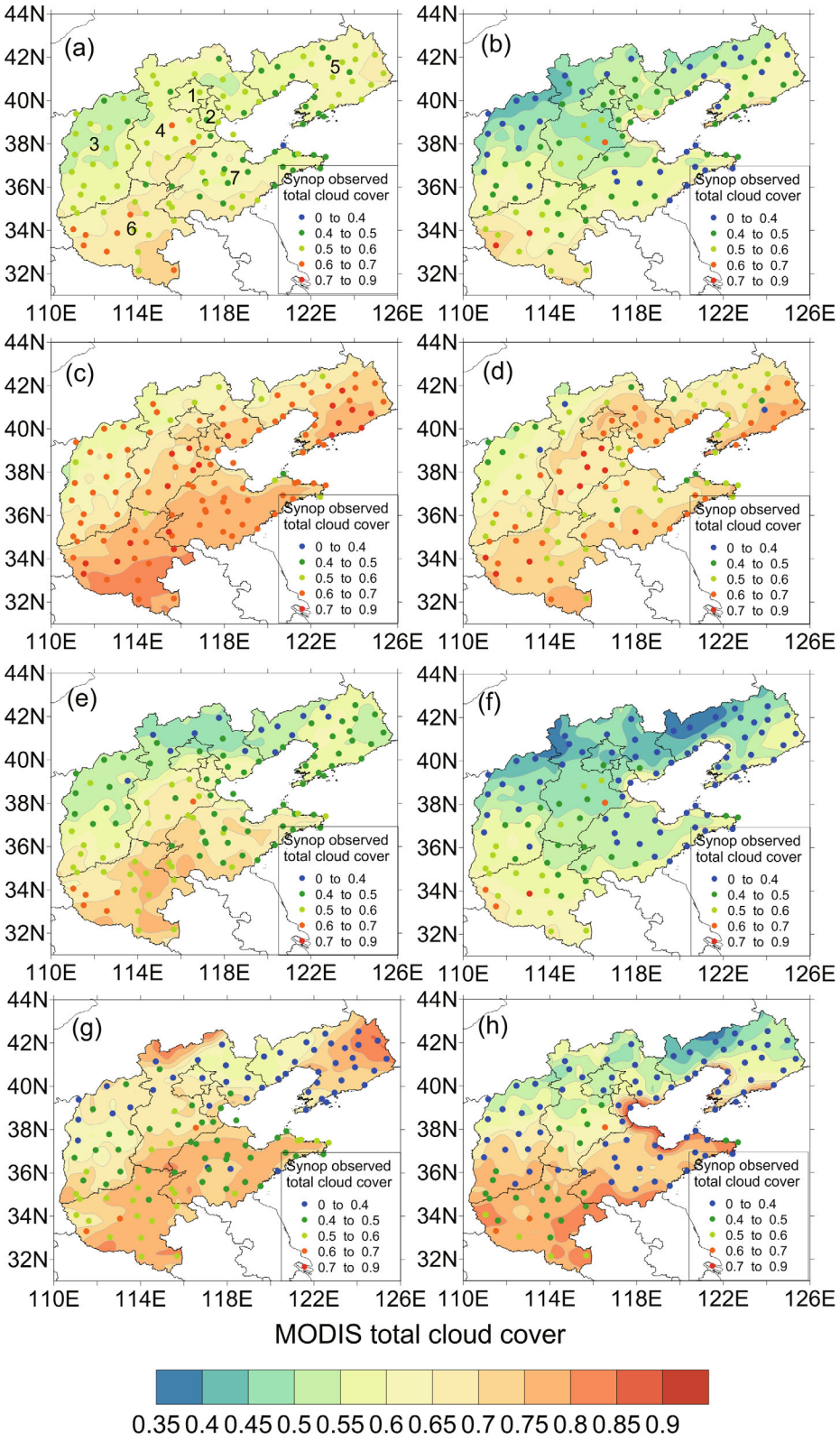

Fig. 2. Climatology of TCC of Aqua MODIS and Synop observations calculated by Aqua MODIS and Synop observations: (a, c, e, g) daytime distribution calculated by observations between December 2002 and November 2013; (b, d, f, h) nighttime distribution calculated by observations between December 2002 and November 2009. Colors of the dots indicate the time-averaged TCC observed by each station. Shading indicates the time-averaged TCC observed by Aqua MODIS. Numbers in (a) represent different regions, 1 for Beijing, 2 for Tianjin, 3 for Shanxi, 4 for Hebei, 5 for Liaoning, 6 for Henan, 7 for Shandong.

was high both in daytime and at nighttime, while the Synop observation was relatively low.

3.2. *Comparison between TCC from Terra and Aqua MODIS*

We conducted a detailed 11-year (December 2002–November 2013) comparison between the MODIS-derived TCC from the Terra and Aqua satellites. Figure 3 compares the monthly averaged TCC observed by Aqua and Terra for all stations. The correlation coefficient (R) between the TCC derived from Terra MODIS and Aqua MODIS was 0.77 for daytime and 0.72 for nighttime, suggesting that Terra MODIS and Aqua MODIS were highly coherent. The Aqua MODIS observation results were slightly larger than those of Terra MODIS for both daytime and nighttime. This may be affected by the satellites' different overpass times.

3.3. *Comparison between daily MODIS and Synop observations*

A comparison between the MODIS and Synop TCC was conducted daily during the period December 2002–November 2013, and the statistical results are shown in Fig. 4 and Table 1. The positive differences between the MODIS and Synop observations were significantly more than the negative ones, and 55% of all differences during daytime and 50% of all differences at nighttime ranged from 0% to 20% (Fig. 4), indicating that the MODIS-observed data were generally greater than the Synop data. The mean difference (D_{ms}) between the MODIS- and Synop-observed data was 13.95% for Terra and 15.25% for Aqua (Table 1).

Table 1 explicitly shows that the deviation at nighttime was greater than that during daytime. The D_{ms} at nighttime was 2% to 3% higher than that during daytime, and the RMSE at nighttime was 3% to 4% higher than during daytime. The R during daytime was 0.69 and 0.67 for Terra and Aqua, respectively, which was higher than the R at nighttime (0.65 and 0.64). This may be affected by the lack of a visible channel, which would reduce the accuracy of the MODIS observation (Kotarba, 2009).

3.4. *Seasonal variations between MODIS and Synop TCC*

The difference between MODIS and Synop TCC also varied with season (Table 2). As shown in Table 2, the deviation between the two datasets was greatest in winter. In winter,

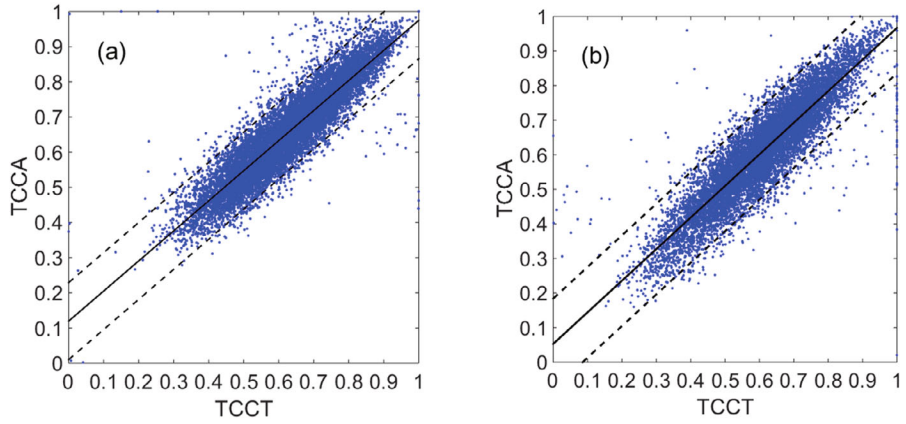

Fig. 3. Difference between TCC observed by Terra MODIS (TCCT) and Aqua MODIS (TCCA) (a) during daytime and (b) at nighttime. Each dot represents a comparison of the average value of Terra and Aqua MODIS in one month at a single station. The solid line is the regression line, while the dashed lines represent the 95% confidence intervals.

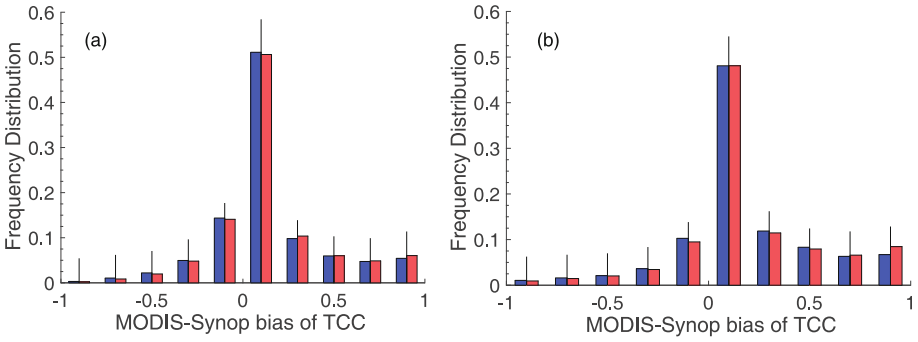

Fig. 4. Frequency distribution of the deviation of MODIS- and Synop-observed TCC at intervals of 0.2 (a) during daytime over 11 years from December 2002 to November 2013, and (b) at nighttime over 7 years from December 2002 to November 2009, for 121 Synop stations. The blue bars on the left represent the deviation between Terra and Synop observations, and the red bars on the right represent the deviation between Aqua and Synop observations.

Table 1. Comparisons of daily TCC observed by MODIS with Synop observations during the period from December 2002 to November 2013 for daytime and December 2002 to November 2009 for nighttime.

	Day (1 Dec. 2002 to 30 Nov. 2013)		Night (1 Dec. 2002 to 30 Nov. 2009)		Day + Night (1 Dec. 2002 to 30 Nov. 2009)	
	Terra	Aqua	Terra	Aqua	Terra	Aqua
Mean difference (%)	12.74	14.14	15.58	16.64	13.95	15.25
RMSE (%)	33.84	34.66	36.96	39.02	35.04	36.20
Correlation coefficient	0.69	0.67	0.65	0.64	0.67	0.65
Number of observations	347 248	446 500	68 125	91 541	136 138	183 106

Table 2. Comparisons of daily MODIS TCC and Synop observations for four seasons during the period from December 2002 to November 2013 for daytime and December 2002 to November 2009 for nighttime.

		Spring (March-May)		Summer (June-August)		Autumn (September-November)		Winter (December in the last year–February in the present year)	
	Parameter	Terra	Aqua	Terra	Aqua	Terra	Aqua	Terra	Aqua
Mean difference(%)	Day	7.70	8.44	2.31	4.29	12.97	14.66	29.42	29.60
	Night	11.98	13.04	6.97	7.99	10.68	12.46	30.15	32.94
	Day + Night	9.64	10.75	4.46	6.07	11.63	13.64	29.53	31.07
RMSE (%)	Day	30.05	30.33	25.13	24.86	32.14	33.62	45.75	46.51
	Night	33.96	36.07	32.85	33.72	33.59	34.01	47.05	49.26
	Day + Night	31.85	32.25	28.69	29.47	32.36	33.78	46.42	47.59
Correlation coefficient	Day	0.75	0.74	0.78	0.76	0.74	0.72	0.59	0.57
	Night	0.71	0.69	0.67	0.65	0.73	0.72	0.54	0.52
	Day + Night	0.72	0.71	0.73	0.71	0.73	0.71	0.56	0.55
Number of observations	Day	87 099	112 657	90 797	112 211	87 499	112 365	81 853	109 267
	Night	15 867	23 483	16 864	23 451	18 356	21 675	17 126	22 843
	Day + Night	31 726	46 745	33 704	46 894	36 707	43 302	34 241	45 639

the D_{ms} and RMSE were the largest among the four seasons; the D_{ms} reached 29.53% and 31.07% and the RMSE 46.42% and 47.59% for Terra and Aqua, respectively. Meanwhile, the R in winter was smallest among the four seasons, being only 0.56 and 0.55 for Terra and Aqua, respectively. The R was similar to a comparison of MODIS and Synop TCC in Poland; however, the D_{ms} was much higher than that in Poland, which was 7.28% in January 2004 (Kotarba, 2009).

In contrast, the difference between the MODIS and Synop TCC was smallest and most consistent in summer. Both the D_{ms} (2.31%–7.99%) and RMSE (24.86%–33.72%) were much smaller than in the other three seasons, and the R was relatively high (0.65–0.78). The mean D_{ms} during daytime and at nighttime in our study regions was 4.46% for Terra and 6.07% for Aqua, which is comparable to the 4.38% in Poland in July 2004 (Kotarba, 2009). Previous research in China found similar results. Ma et al. (2014) found that the D_{ms} calculated by full-year data was 15.09% in North China, while the D_{ms} decreased to 5.29% after removal of the winter data. Lu et al. (2015) found that in the China area the correlation between the two observation results was highest in summer (0.736) and lowest in winter (0.667).

The deviation between MODIS and Synop TCC in spring and autumn was between that of summer and winter, and did not show any great difference. The high R, ranging from 0.69 to 0.75, suggested good consistency between MODIS and Synop TCC. Table 2 shows that in all seasons the D_{ms} and RMSE during daytime were much smaller than at nighttime and the R during daytime was much higher than that at nighttime, indicating that the TCC observed during daytime was much better than that at nighttime.

3.5. *Relationship between the cloud fraction deviation and CTH/COT*

Considering different cloud types may influence both MODIS and Synop observations and further influence the D_{ms}, two physical characteristics—CTH and COT, which are important parameters to distinguish different cloud types—were chosen to discuss their relationship with D_{ms}. Because of the lack of COT observations at night, both discussions focus on the data during daytime only.

Figure 5a shows the average CTH under different D_{ms} levels. It can be clearly seen from the figure that when the D_{ms} was less than zero the average CTH was at a relatively

high value. In the area that the D_{ms} was near zero the average CTH was at a peak. Meanwhile, when the D_{ms} was greater than 0.2 the CTH showed a sharp decrease with an increase in the D_{ms}. When the D_{ms} was close to 1 the average CTH was near 1 km.

Figure 5b facilitates further discussion on the D_{ms} distribution for clouds with different CTH. The figure shows that under conditions with lower CTH the distribution frequency of bigger D_{ms} was much higher, and D_{ms} values greater than 0.2 mainly appeared when CTH was less than 2 km. With an increase in CTH the proportion of bigger D_{ms} values reduced rapidly. This result shows that MODIS more easily detects cloud with low CTH, which Synop observations were otherwise unable to detect.

The other characteristic, COT, is discussed based on the results in Fig. 6. Figure 6a shows that the average COT with D_{ms} near zero was obviously higher. In contrast, the average COT with deviation larger than 0.2 was generally low in value. The distribution of D_{ms} under different COT is presented in Fig. 6b. As can be seen in the figure, large deviation mainly occurred under conditions with low COT. When COT was greater than 20, nearly all deviations were smaller than 0.2.Meanwhile, when COT was smaller than 12, the frequency of deviations greater than 0.2 was nearly half.

It can be inferred from the analysis above that MODIS tends to detect cloud with low CTH and small COT that is otherwise undetected by Synop observations, meaning there may be cases that Cu and Sc clouds are detected by MODIS but undetected or underestimated by Synop observations. Given that previous research has proven that MODIS tends to judge the layer of aerosols at low altitude as cloud (Shang et al., 2014; Mao et al., 2015), it is possible that MODIS in the present study judged the aerosol layer as cloud, leading to the high D_{ms}. Another possibility is that the surface FOV was larger for high cloud; surface observations can see high cloud in a larger radius than low cloud, which increases the surface-observed high cloud fraction.

3.6. *Possible reasons for the difference between MODIS and Synop*

To explore the possible factors influencing the consistency and deviation between MODIS and Synop TCC observations, we analyzed the relationship between the deviation with AOD, VZA, and snow cover.

The averaged D_{ms} in different VZA intervals (Fig. 7a) showed that the deviation of TCC increased with an increase in VZA. Under conditions of VZA < 30°, the D_{ms} basically maintained at a low level (< 7%); whereas, at VZA > 30°, the D_{ms} increased systematically with VZA. The averaged D_{ms} at the largest VZA interval (23.45%) was 19.68% greater than

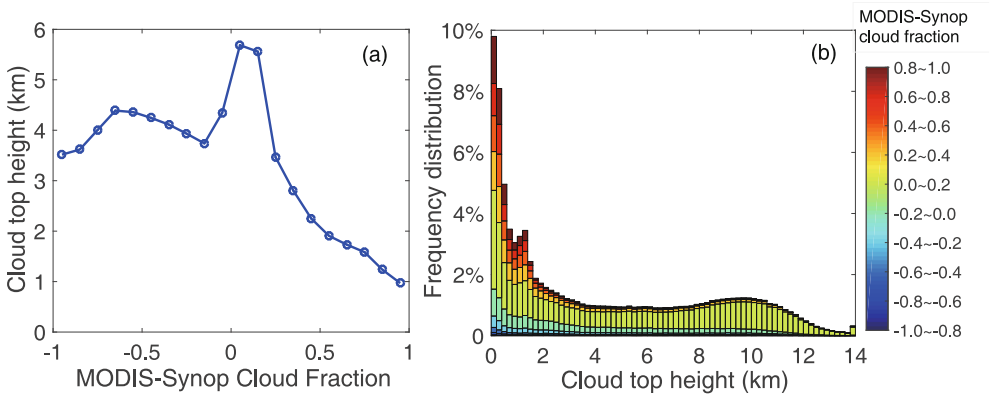

Fig. 5. (a) Average CTH under conditions of different D_{ms}. (b) Cumulative frequency distribution of D_{ms} under different CTH at intervals of 200 m.

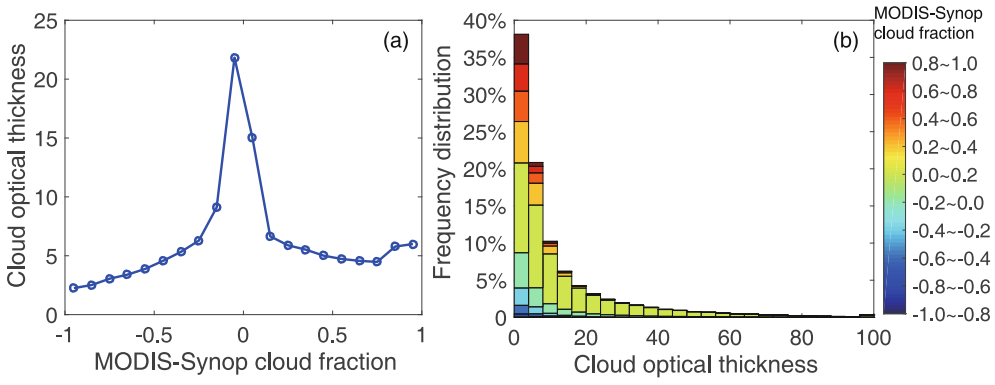

Fig. 6. (a) Average COT under conditions of different D_{ms}. (b) Cumulative frequency distribution of D_{ms} under different COT at intervals of 4.

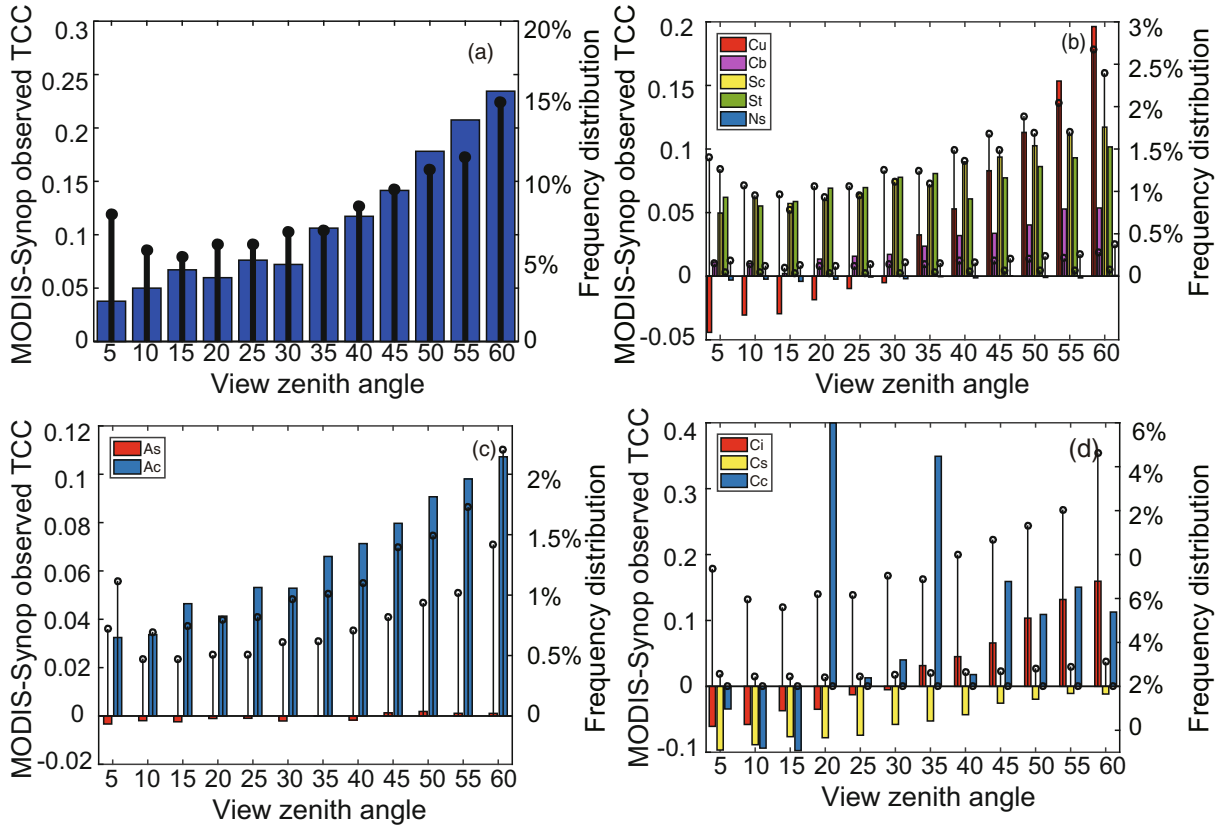

Fig. 7. Average D_{ms} calculated for different cloud types under conditions of different VZA at interval of 5°. Each bar color represents a cloud type (see legend). The stems of each colored bar represent the VZA frequency distribution.

the D_{ms} at the smallest VZA interval (3.77%). The regression result also showed that larger VZA would lead to larger MODIS observations. This is consistent with previous studies (Maddux et al., 2010; An and Wang, 2015). The larger VZA would decrease the clear space between clouds, especially for thick clouds like convective clouds, on account of the vertical sides of the clouds would be viewed by the satellite. This effect was especially obvious for convective clouds or broken clouds. Another possible reason was that pixels with larger VZA have larger size and longer observation path lengths, which may increase the satellite-observed TCC.

Analysis of the relationships between cloud types and VZA (Figs. 7b–d) showed that high VZA would lead to the D_{ms} of most categories of clouds being higher when the VZA was higher. Besides, observations of broken clouds were more likely to be affected by the VZA. Cu, Cb and Ac showed significant increasing trend as the VZA became larger. In contrast, cloud covering the whole sky had a relative stable observation result. The trends of Sc, St, Ns and As were not as obvious as the other types of cloud. It is worth noting that the D_{ms} of most cloud types was positive, while that of Ns and As was near zero, possibly because both MODIS and Synop observations were near to 1 under these conditions; plus, Cs was negative in every VZA, which was possibly because MODIS had a relative weak detection ability for thin ice cloud, as proven by Holz et al. (2008).

Figure 8 shows the spatial distribution of Aqua MODIS AOD and the averaged D_{ms} between MODIS and Synop at each Synop station in the four seasons. Because of the lack of AOD observations at nighttime, only observations during daytime were analyzed. The D_{ms} was averaged from the D_{ms} of Terra and Aqua MODIS. In all seasons, the distribution of the averaged D_{ms} was consistent with the distribution of AOD. Stations with low D_{ms} values mainly distributed in the northwestern area and Shandong's coastal area, which were the low AOD value areas. In contrast, the D_{ms} in central and western Shandong, central and eastern Henan, as well as southern Hebei, were generally higher than in other areas.

Note that in the Liaoning area the D_{ms} was slightly larger than in areas with the same AOD value (Fig. 8). This phenomenon became quite obvious in winter (Fig. 8d). In winter, the D_{ms} in Liaoning was even larger than that in the border regions of Shandong, Hebei and Henan, where AODs were largest. This might be influenced by snow cover and the low solar height angle due to Liaoning being located at high latitudes.

To further investigate the impact of AOD on the difference between satellite and Synop TCC observations for each cloud type, the D_{ms} values at different AOD intervals were calculated (Fig. 9). Figure 9a shows that the D_{ms} was greater at high AODs. In all seasons, the D_{ms} tended to increase generally with an increase in AOD. In summer, the D_{ms} increased monotonically with increasing AOD over the entire AOD range. In spring, autumn and winter, the D_{ms} increased

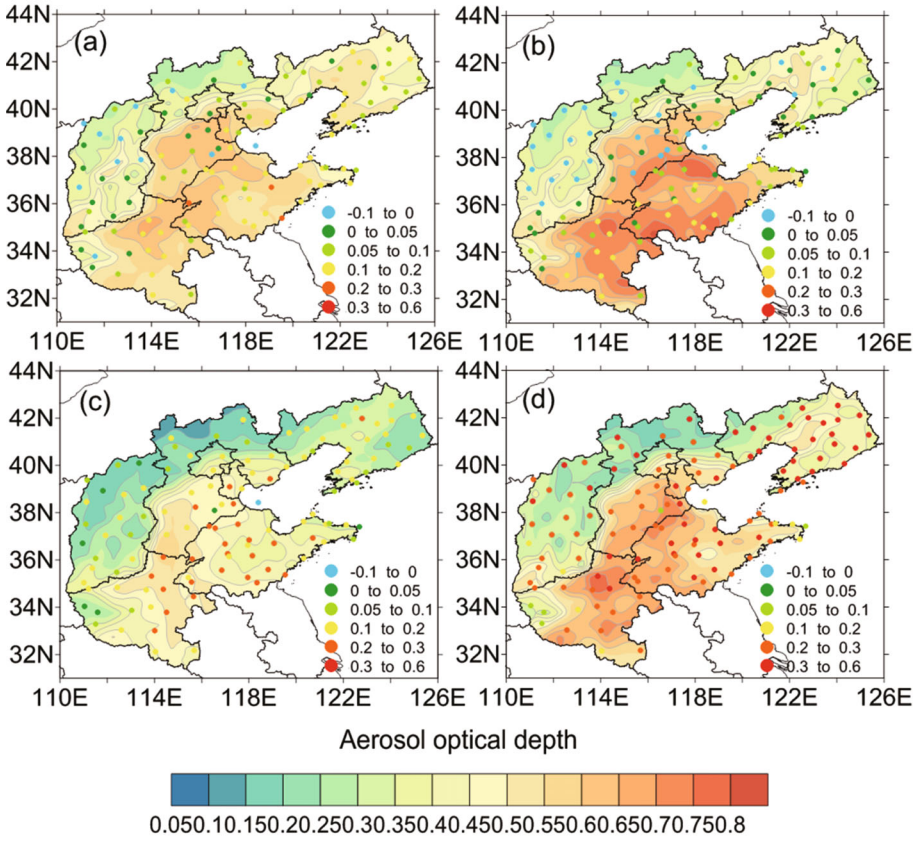

Fig. 8. D_{ms} of TCC in (a) spring, (b) summer, (c) autumn and (d) winter. Color of each dot indicates the time-averaged deviation level of each station. Shading indicates the time-averaged Aqua MODIS AOD at 550 nm.

with AOD values at AOD < 1.5, whereas the D_{ms} showed no remarkable change and even dropped slightly with increasing AOD at AOD > 1.5. That may have been caused by a small amount of high AODs (Fig. 9) or the environment was not so different to satellite and visual surface observations at AOD > 1.5.

Analysis of different cloud types (Figs. 9b–d) showed that the D_{ms} of most cloud types increased with AOD. The most obvious were Cu, Ac, Ci and Cs, which did not cover the whole sky. Misjudging the aerosol layer as cloud by MODIS may be the reason behind this phenomenon.

To further investigate the influence of snow cover, the relationship between snow cover and the D_{ms} in winter is shown in Fig. 10. The distribution of D_{ms} values showed consistency with the distribution of snow cover. In winter, the main areas with high D_{ms} values appeared in the provinces of Liaoning and Shandong. The above analysis shows that high AODs in Shandong induced high D_{ms} values; however, Liaoning had much lower AOD values. The large snow coverage in Liaoning may have resulted in the higher D_{ms}.

4. Summary

This study compared MODIS (Terra and Aqua) and Synop surface observed cloud fraction over the NCP and its surrounding regions during the period from December 2002 to November 2013 during daytime, and from December 2002 to November 2009 at nighttime. The comparison showed that certain differences existed between MODIS- and Synop-observed TCC. MODIS observed a significantly higher value, and this phenomenon was more obvious at nighttime. At nighttime, the mean difference between Synop and Terra/Aqua MODIS was 15.58% and 16.64%, respectively; and this was greater than during daytime, being 12.74% and 14.14% for Terra and Aqua, respectively. The regression correlation coefficient between Synop and Terra/Aqua MODIS at nighttime was 0.65 and 0.64, respectively, which was smaller than during daytime (0.69 and 0.67 for Terra and Aqua, respectively). The comparison also revealed considerable changes in different seasons. The mean differences for Terra MODIS and Aqua MODIS in winter (29.53% and 31.07%, respectively) were much higher than in the other three seasons (ranging from 4.46% to 13.64%), and the correlation coefficients in winter (0.56 and 0.55 for Terra and Aqua, respectively) were less than in the other three seasons (ranging from 0.71 to 0.73).

Analysis of the effect of cloud characteristics on the observational deviation found that CTH and COT had an obvious influence on D_{ms}. Cloud with low CTH was more likely to cause a higher MODIS observational result and lower

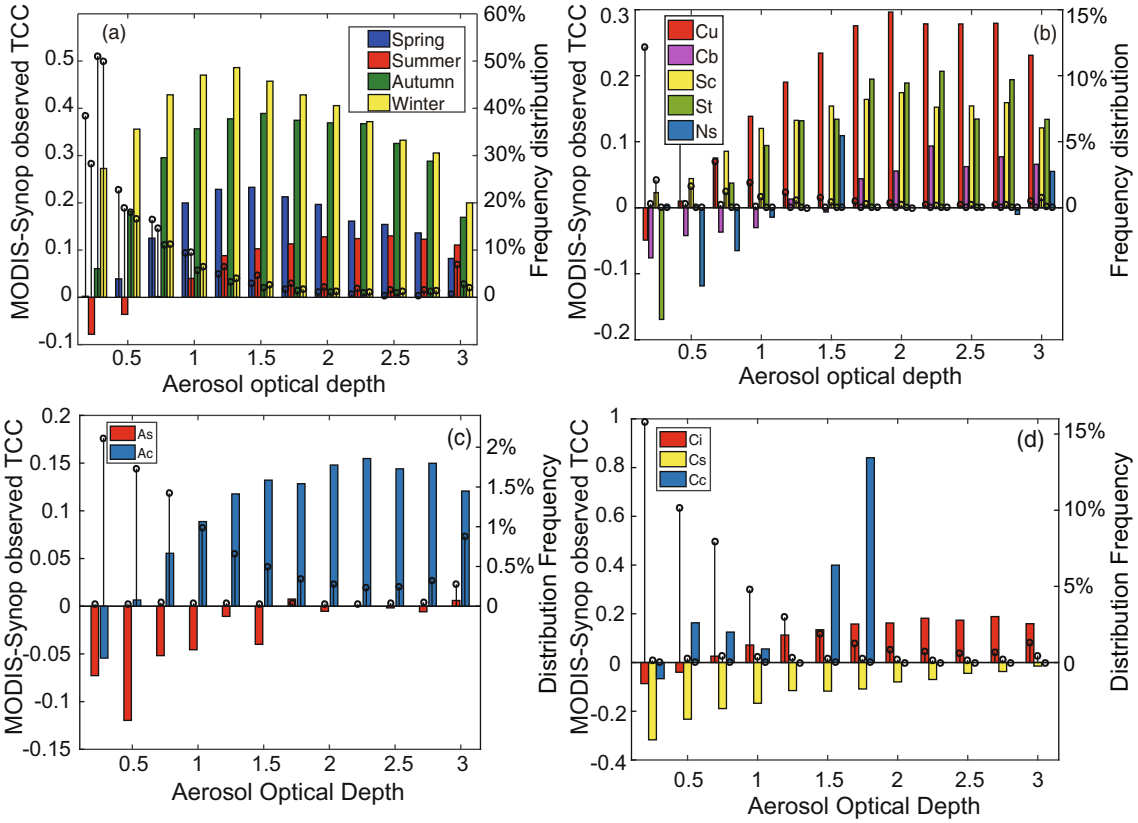

Fig. 9. Average D_{ms} calculated for different (a) seasons and (b–d) cloud types under conditions of different AOD at intervals of 0.25. Each bar color represents a cloud type (see legend). The stems marked in the middle of each colored bar represent the AOD frequency distribution, corresponding to the ticks of the right-hand *y*-axis.

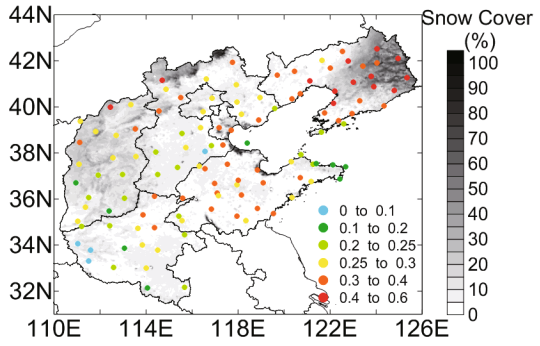

Fig. 10. Difference between MODIS- and Synop-observed TCC in winter. Color of each dot represents the deviation level of each station. The shading indicates the snow coverage.

Synop observational result, while this frequency reduced significantly when the CTH was lower than 4 km. Another point is that observations with significant deviations mainly occurred when COT was less than 12.

Analysis showed that a large VZA would lead to a larger MODIS-observed TCC, and this effect was more obvious for clouds occurring in clumps than cloud covering the whole sky. Besides, thin clouds like Cs would lead to a negative D_{ms}, and a high VZA value would improve the MODIS detection. Similar results were seen for the effect of AOD. The spatial distribution of the difference between MODIS and Synop matched well with the AOD distribution, and the difference increased with an increase in AOD. The difference in the NCP and its surrounding regions was higher than that in Poland, Europe (Kotarba, 2009), suggesting that high pollution may induce a greater MODIS TCC. In addition, high snow coverage may affect MODIS observations, thus resulting in a high difference in northern areas.

Acknowledgements. This work was supported by the National Natural Science Foundation of China (Grant Nos. 41590874 and 41590875) and the Ministry of Science and Technology of China (Grant No. 2014CB953703). The MODIS cloud and aerosol properties were provided by the Level 1 and Atmosphere Archive and Distribution System of the NASA Goddard Space Flight Center. We are grateful to the China Meteorological Administration for providing the visual surface cloud cover data.

REFERENCES

An, N., and K. C. Wang, 2015: A comparison of MODIS-derived cloud fraction with surface observations at five SURFRAD sites. *Journal of Applied Meteorology and Climatology*, **54**, 1009–1020, https://doi.org/10.1175/JAMC-D-14-0206.1.

Bilal, M., and J. E. Nichol, 2015: Evaluation of MODIS aerosol retrieval algorithms over the Beijing-Tianjin-Hebei region dur-

ing low to very high pollution events. *J. Geophys. Res*., **120**, 7941–7957, https://doi.org/10.1002/2015JD023082.

Che, H., and Coauthors, 2014: Column aerosol optical properties and aerosol radiative forcing during a serious haze-fog month over North China Plain in 2013 based on ground-based sunphotometer measurements. *Atmos. Chem. Phys.*, **14**, 2125–2138, https://doi.org/10.5194/acp-14-2125-2014.

Che, H. Z., G. Y. Shi, X. Y. Zhang, R. Arimoto, J. Q. Zhao, L. Xu, B. Wang, and Z. H. Chen, 2005: Analysis of 40 years of solar radiation data from China, 1961-2000. *Geophys. Res. Lett*., **32**, L06803, https://doi.org/10.1029/2004GL022322.

Che, H. Z., X. Y. Zhang, Y. Li, Z. J. Zhou, and J. J. Qu, 2007: Horizontal visibility trends in China 1981-2005. *Geophys. Res. Lett*., **34**, L24706, https://doi.org/10.1029/2007GL031450.

Chen, H. P., and H. J. Wang, 2015: Haze Days in North China and the associated atmospheric circulations based on daily visibility data from 1960 to 2012. *J. Geophys. Res*., **120**, 5895–5909, https://doi.org/10.1002/2015JD023225.

CMDSSS, 2009: China Meteorological Data Sharing Service System. China Meteorological Administration, Beijing, China. [Available at http://www.cma.gov.cn.]

Dybbroe, A., K.-G. Karlsson, and A. Thoss, 2005: NWCSAF AVHRR cloud detection and analysis using dynamic thresholds and radiative transfer modeling. Part I: Algorithm description. *J. Appl. Meteor*., **44**, 39–54, https://doi.org/10.1175/JAM-2188.1.

Feister, U., H. Möller, T. Sattler, J. Shields, U. Görsdorf, and J. Güldner, 2010: Comparison of macroscopic cloud data from ground-based measurements using VIS/NIR and IR instruments at Lindenberg, Germany. *Atmos. Res.*, **96**, 395–407, https://doi.org/10.1016/j.atmosres.2010.01.012.

Fontana, F., D. Lugrin, G. Seiz, M. Meier, and N. Foppa, 2013: Intercomparison of satellite- and ground-based cloud fraction over Switzerland (2000-2012). *Atmos. Res.*, **128**, 1–12, https://doi.org/10.1016/j.atmosres.2013.01.013.

Green, M., S. Kondragunta, P. Ciren, and C. Y. Xu, 2009: Comparison of GOES and MODIS aerosol optical depth (AOD) to aerosol robotic network (AERONET) AOD and IMPROVE $PM_{2.5}$mass at Bondville, Illinois. *Journal of the Air & Waste Management Association*, **59**, 1082–1091, https://doi.org/10.3155/1047-3289.59.9.1082.

Hahn, C. J., S. G. Warren, and J. London, 1992: The effect of moonlight on observation of cloud cover at night, and application to cloud climatology. *J. Climate*, **8**,1429–1446, https://doi.org/10.1175/1520-0442(1995)008<1429:TEOMOO>2.0.CO;2.

Hall, D. K., G. A. Riggs, and V. Salomonson, 2006: MODIS snow and sea ice products. *Earth Science Satellite Remote Sensing*, Qu et al., Eds., Springer, Berlin Heidelberg, 154–181, https://doi.org/10.1007/978-3-540-37293-6_9.

Heidinger, A. K., V. R. Anne, and C. Dean, 2002: Using MODIS to estimate cloud contamination of the AVHRR data record. *J. Atmos. Oceanic Technol*, **19**, 586–601, https://doi.org/10.1175/1520-0426(2002)019<0586:UMTECC>2.0.CO;2.

Holz, R. E., S. A. Ackerman, F. W. Nagle, R. Frey, S. Dutcher, R. E. Kuehn, M. A. Vaughan, and B. Baum, 2008: Global moderate resolution imaging spectro radiometer (MODIS) cloud detection and height evaluation using CALIOP. *J. Geophys. Res*., **113**, D00A19, https://doi.org/10.1029/2008JD009837.

Hsu, N. C., S. C. Tsay, M. D. King, and J. R. Herman, 2004: Aerosol properties over bright-reflecting source regions. *IEEE Transactions on Geoscience and Remote Sensing*, **42**, 557–569, https://doi.org/10.1109/TGRS.2004.824067.

Huo, J., and D. R. Lu, 2012: Comparison of cloud cover from all-sky imager and meteorological observer. *J. Atmos. Oceanic Technol*., **29**, 1093–1101, https://doi.org/10.1175/JTECH-D-11-00006.1.

Kästner, M., P. Bissolli, and K. Hoppner, 2004: Comparison of a satellite based Alpine cloud climatology with observations of synoptic stations. *Meteor. Z*., **13**, 233–243, https://doi.org/10.1127/0941-2948/2004/0013-0233.

Kazantzidis, A., P. Tzoumanikas, A. F. Bais, S. Fotopoulos, and G. Economou, 2012: Cloud detection and classification with the use of whole-sky ground-based images. *Atmos. Res.*, **113**, 80–88, https://doi.org/10.1016/j.atmosres.2012.05.005.

Key, E. L., P. J. Minnett, and R. A. Jones, 2004: Cloud distributions over the coastal Arctic Ocean: Surface-based and satellite observations. *Atmos. Res*., **72**, 57–88, https://doi.org/10.1016/j.atmosres.2004.03.029.

Kotarba, A. Z., 2009: A comparison of MODIS-derived cloud amount with visual surface observations. *Atmos. Res.*, **92**, 522–530, https://doi.org/10.1016/j.atmosres.2009.02.001.

Kotarba, A. Z., 2015: Evaluation of ISCCP cloud amount with MODIS observations. *Atmos. Res.*, **153**, 310–317, https://doi.org/10.1016/j.atmosres.2014.09.006.

Levy, R. C., L. A. Remer, and O. Dubovik, 2007a: Global aerosol optical properties and application to Moderate Resolution Imaging Spectro radiometer aerosol retrieval over land. *J. Geophys. Res*., **112**, D13210, https://doi.org/10.1029/2006JD007815.

Levy, R. C., L. A. Remer, S. Mattoo, E. F. Vermote, and Y. J. Kaufman, 2007b: Second-generation operational algorithm: Retrieval of aerosol properties over land from inversion of Moderate Resolution Imaging Spectro radiometer spectral reflectance. *J. Geophys. Res*., **112**, D13211, https://doi.org/10.1029/2006JD007811.

Levy, R. C., S. Mattoo, L. A. Munchak, L. A. Remer, A. M. Sayer, and N. C. Hsu, 2013: The Collection 6 MODIS aerosol products over land and ocean. *Atmospheric Measurement Techniques Discussions*, **6**, 159–259, https://doi.org/10.5194/amtd-6-159-2013.

Li, X. Y., 2016: Empirical analysis of the smog factors in Beijing-Tianjin-Hebei region. *Ecological Economy*, **32**, 144–150, https://doi.org/10.3969/j.issn.1671-4407.2016.03.029. (in Chinese)

Li, Z., and Coauthors, 2013: Aerosol physical and chemical properties retrieved from ground-based remote sensing measurements during heavy haze days in Beijing winter. *Atmos. Chem. Phys.*, **13**, 10 171–10 183, https://doi.org/10.5194/acp-13-10171-2013.

Liang, F., and X. A. Xia, 2005: Long-term trends in solar radiation and the associated climatic factors over China for 1961-2000. *Annales Geophysicae*, **23**, 2425–2432, https://doi.org/10.5194/angeo-23-2425-2005.

Lu, H., Y. W. Zhang, and J. Cai, 2015: Consistency and differences between remotely sensed and surface observed total cloud cover over China. *Int. J. Remote Sens*., **36**, 4160–4176, https://doi.org/10.1080/01431161.2015.1072651.

Luo, Y. F., D. R. Lu, X. J. Zhou, W. L. Li, and Q. He, 2001: Characteristics of the spatial distribution and yearly variation of aerosol optical depth over China in last 30 years. *J. Geophys. Res*., **106**, 14 501–14 513, https://doi.org/10.1029/2001JD900030.

Ma, J. J., H. Wu, C. Wang, X. Zhang, Z. Q. Li, and X. H.

Wang, 2014: Multiyear satellite and surface observations of cloud fraction over China. *J. Geophys. Res*., **119**, 7655–7666, https://doi.org/10.1002/2013JD021413.

Maddux, B. C., S. A. Ackerman, and S. Platnick, 2010: Viewing geometry dependencies in MODIS cloud products. *J. Atmos. Oceanic Technol*., **27**, 1519–1528, https://doi.org/10.1175/2010JTECHA1432.1.

Mao, F. Y., M. M. Duan, Q. L. Min, W. Gong, Z. X. Pan, and G. Y. Liu, 2015: Investigating the impact of haze on MODIS cloud detection. *J*. *Geophys*. *Res*., **120**,12 237–12 247, https://doi.org/10.1002/2015JD023555.

Meerkötter, R., C. König, P. Bissolli, G. Gesell, and H. Mannstein, 2004: A 14-year European Cloud Climatology from NOAA/AVHRR data in comparison to surface observations. *Geophys*. *Res*. *Lett*., **31**,L15103, https://doi.org/10.1029/2004GL020098.

Menzel, W. P., and Coauthors, 2008: MODIS global cloud-top pressure and amount estimation: Algorithm description and results. *Journal of Applied Meteorology and Climatology*, **47**, 1175–1198, https://doi.org/10.1175/2007JAMC1705.1.

Minnis, P., D. A. Spangenberg, and V. Chakrapani, 2003: Distribution and validation of cloud cover derived from AVHRR data over the Arctic Ocean during the SHEBA year. *Proceedingsofthe13thARMScienceTeamMeeting*, Broomfield, Colorado.

Platnick, S., M. D. King, S. Ackerman, W. P. Menzel, B. A. Baum, J. C. Riédi, and R. A. Frey, 2003: The MODIS cloud products: Algorithms and examples from Terra. *IEEE Transactionson Geoscience and Remote Sensing*, **41**, 459–473, https://doi.org/10.1109/TGRS.2002.808301.

Qiu, J. H., and L. Q. Yang, 2000: Variation characteristics of atmospheric aerosol optical depths and visibility in North China during 1980-1994. *Atmos*. *Environ*., **34**, 603–609, https://doi.org/10.1016/S1352-2310(99)00173-9.

Ramanathan, V.,R. D. Cess, E. F. Harrison, P. Minnis, B. R. Barkstrom, E. Ahmad, and D. Hartmann, 1989: Cloud-radiative forcing and climate: Results from the earth radiation budget experiment. *Science*, **243**, 57–63, https://doi.org/10.1126/science.243.4887.57.

Remer, L. A., and Coauthors, 2005: The MODIS aerosol algorithm, products, and validation. *J. Atmos. Sci*., **62**, 947–973, https://doi.org/10.1175/JAS3385.1.

Rossow, W. B., A. W. Walker, and L. C. Garder, 1993: Comparison of ISCCP and other cloud amounts. *J. Climate*, **6**, 2394–2418, https://doi.org/10.1175/1520-0442(1993)006<2394:COIAOC>2.0.CO;2.

Shang, H. Z., L. F. Chen, J. H. Tao, L. Su, and S. L. Jia, 2014: Synergetic use of MODIS cloud parameters for distinguishing high aerosol loadings from clouds over the North China Plain. *IEEE Journal of Selected Topics in Applied Earth Observations and Remote Sensing*, **7**, 4879–4886, https://doi.org/10.1109/JSTARS.2014.2332427.

Wang, H., G. Y. Shi, X. Y. Zhang, S. L. Gong, S. C. Tan, B. Chen, H. Z. Che, and T. Li, 2015b: Mesoscale modelling study of the interactions between aerosols and PBL meteorology during a haze episode in China Jing-Jin-Ji and its near surrounding region-Part 2: Aerosols' radiative feedback effects. *Atmos. Chem. Phys.*, **15**, 3277–3287, https://doi.org/10.5194/acp-15-3277-2015.

Wang, H., and Coauthors, 2015c: Mesoscale modeling study of the interactions between aerosols and PBL meteorology during a haze episode in Jing-Jin-Ji (China) and its nearby surrounding region-Part 1: Aerosol distributions and meteorological features. *Atmos. Chem. Phys.*, **15**, 3257–3275, https://doi.org/10.5194/acp-15-3257-2015.

Wang, H. J., H. P. Chen, and J. P. Liu, 2015a: Arctic sea ice decline intensified haze pollution in eastern China. *Atmos. Oceanic Sci. Lett.*, **8**, 1–9, https://doi.org/10.3878/AOSL20140081.

Wang, H. J., and Coauthors, 2015d: A review of seasonal climate prediction research in China. *Adv. Atmos. Sci*., **32**, 149–168, https://doi.org/10.1007/s00376-014-0016-7.

Warren, S. G., R. M. Eastman, and C. J. Hahn, 2007: A survey of changes in cloud cover and cloud types over land from surface observations, 1971-96. *J. Climate*, **20**, 717–738, https://doi.org/10.1175/JCLI4031.1.

Xia, X., 2010: A closer looking at dimming and brightening in China during 1961-2005. *Annales Geophysicae*, **28**, 1121–1132, https://doi.org/10.5194/angeo-28-1121-2010.

Zhang, R., and Coauthors, 2013: Chemical characterization and source apportionment of $PM_{2.5}$ in Beijing: Seasonal perspective. *Atmos. Chem. Phys.*, **13**, 7053–7074, https://doi.org/10.5194/acp-13-7053-2013.